25. Suthana N, Fried I. Percepts to recollections: insights from single neuron recordings in the human brain. *Trends Cogn Sci*. 2012;16(8):427-436.
26. Wilke C, Ding L, He B. Estimation of Time-Varying Connectivity Patterns Through the Use of an Adaptive Directed Transfer Function. *Ieee Transactions on Biomedical Engineering*. 2008;55(11):2557-2564.
27. Zhang H, Benz HL, Bezerianos A, et al. Connectivity mapping of the human ECoG during a motor task with a time-varying dynamic Bayesian network. *Conf Proc IEEE Eng Med Biol Soc*. 2010:130-133.
28. Quiroga RQ, Reddy L, Kreiman G, Koch C, Fried I. Invariant visual representation by single neurons in the human brain. *Nature*. 2005;435(7045):1102-1107.
29. Patterson WR, Song YK, Bull CW, et al. A microelectrode/microelectronic hybrid device for brain implantable neuroprosthesis applications. *IEEE Trans Biomed Eng*. 2004;51(10):1845-1853.
30. Polikov VS, Tresco PA, Reichert WM. Response of brain tissue to chronically implanted neural electrodes. *J Neurosci Methods*. 2005;148(1):1-18.

Figure legends

Figure 1. A microwire-combined depth electrode. (A) Electrodedesign. The upper drawing shows a polyamide depth electrode with six platinum contacts and a special inner stylet that can be firmly attached to the pointer probe of the navigation system. The lower drawing shows the eight platinum/iridium microwires. Tips of microwires extend 1.5 to 5 mm beyond the tip of the depth electrode. (B) Low- and high-magnification photographs of electrodes. The upper panel shows the depth electrode with inserted microwires. The special inner stylet is also shown adjacent to the depth electrode. The length of the stylet shaft was equal to that of the depth electrode. The lower panel shows the tip of the wire electrode composed of eight microwires. Scale bars indicate 5 mm. (C) High-magnification view of the depth electrode with silicone fringe. Each silicone fringe was cut into a suitable shape and size. (D) Macroscopic view of the operative field after implantation of all the electrodes except microwires. Black arrowheads indicate depth electrodes inserted to hippocampus. White arrowhead denotes a trapezoid electrode locating the surface of parahippocampal gyrus. Asterisks show grid electrodes implanted to the lateral surface (black) and ventral temporal surface (white). The green dotted line represents the sylvian fissure.

Figure 2. Location of implanted electrodes in a patient with temporal lobe epilepsy. (A) Three-dimensional view of all the electrodes reconstructed from postoperative high-resolution computerized tomography. Asterisks indicate microwire-combined depth electrodes. R, right. (B) Three-dimensionally rendered MRI figures showing the location of microwire-combined depth electrodes in co-registered high-resolution computerized tomography. Axial and

coronal views of the electrodes targeted to the hippocampal head (top) and the subiculum (bottom). Yellow lines indicate the positions of the coronal sections shown in the right panel. Green dots denote the contacts of depth electrodes. (C) Left:axial view of planned and inserted trajectories. Green dotted lines show actually inserted electrodes while white lines represent planned trajectories. Right:high-magnification view measuring the gap between the target point and implanted point.

Figure 3. Spatial errors between the target point and implanted point. Each panel represents a three-dimensional display (upper left), Y-Z axis (upper right), X-Z axis (lower left) and X-Y axis (lower right), respectively. Center cross indicates target; circles show the actual position of the implanted electrodes.

Figure 4. Temporal stability of successful recording rate. 11-15 days after surgery showed the highest performance (mean: 13.6%) and 6-10 days showed the lowest (mean: 8.2%), respectively. No significant difference was observed among each recording period ($P = 0.65$; Kruskal-Wallis test). Bars show the standard deviations.

Figure 5. Comparison among single-unit firing rate (top), LFP (2^{nd} row), raw iEEG (3^{rd} row) and power spectrogram calculated from iEEG (bottom). X-axis represents time from clinical seizure onset. Spikes and LFP were recorded with the microwire placed in the right hippocampal head, and iEEG was recorded from the nearest electrode that covered the medial parahippocampalgyrus. Red dashed line represents clinical seizure onset. ERSP: event-related spectral perturbation.

Figure 6. Peristimulus-timehistograms of hippocampal neuron activityof a patient in response to visual presentation of photographs of close family members. 1^{st} column representthe firing rate for visual stimuli of family 1. 2^{nd}, 3^{rd} and 4^{th} column indicate the responses to the photographs of family 2, 3 and 4, respectively. X-axis represents time from visual stimulus onset, and Y-axis represents summated firing rate of 38 trials within the temporal 100-ms time bin. Dashed vertical lines indicate the onset and offset of visual stimulation (1-sec. presentation). Dashed horizontal lines in red indicate mean + 2 SD level of the spontaneous firing rate.

Table 1. Summary of patient characteristics

Subject	Age/sex	Num. of depth electrode (grid/strip electrode)	Laterality	Location	MRI findings	Successful recording
1	22 / F	2 (204)	L	H / S	L. hippocampal sclerosis	1/8
2	24 / M	4 (236)	L	H / S	L. cortical dysplasia	3/16
3	30 / M	2 (196)	L	H / Trigonum	L. periventricular nodular heterotopia	0 / 16
4	41 / F	4 (248)	B	H / S	Non-lesional	1/32
5	23 / M	2 (83)	L	Parietal	Non-lesional	1/ 16
6	37 / M	4 (198)	B	H / S	L. hippocampal sclerosis	6/32
7	35 / F	4 (210)	B	H / S	Non-lesional	0 /32
8	38 / F	4 (242)	B	H / S	Non-lesional	13 /32
9	15 / M	4 (158)	B	H / S	R. temporal cystic tumor	6 /32

Table 1. Summary of electrode number/location, MRI findings and clinical data. Subject 7 was excluded from data analysis because of damage to the ground/reference wire.L, left; R, right; B, bilateral; H, hippocampus; S, subiculum.

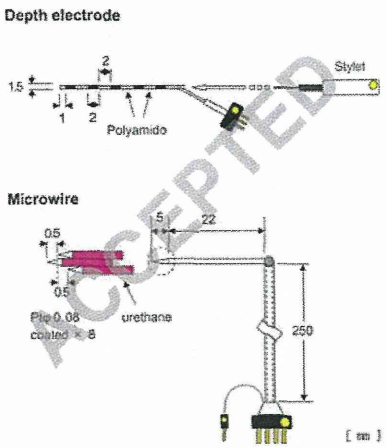
Depth electrode
2
1.5
1
2
Polyamido
Stylet
Microwire
1.5
22
0.5
0.5
Pte 0.08
coated
urethane
250
[mm]

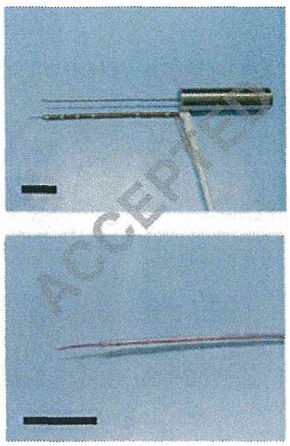

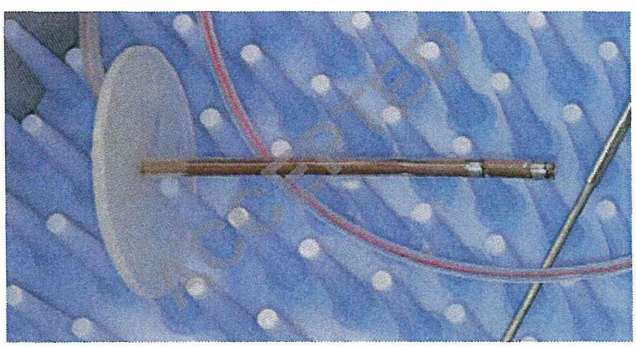

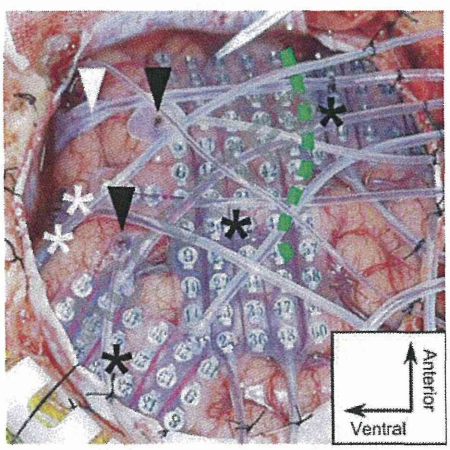
Anterior
Ventral

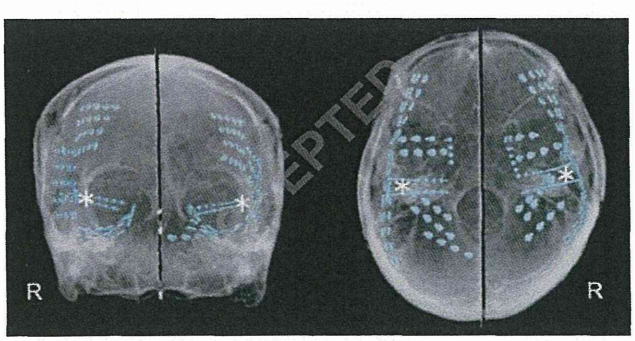
R
R

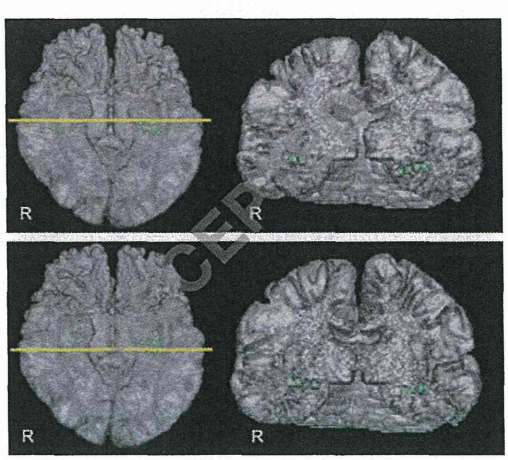
R
R
R
R

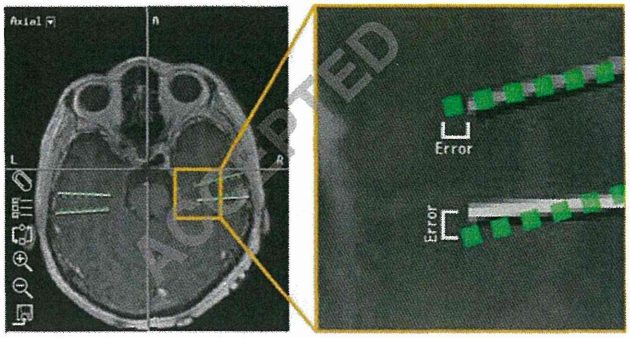
Axial
Error
Error

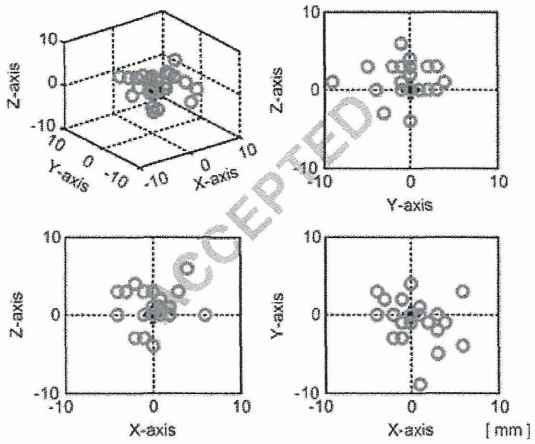
Z-axis
Y-axis
X-axis
[mm]

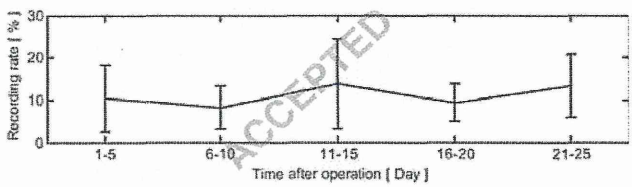
Recording rate [%]
1-5
6-10
11-15
16-20
21-25
Time after operation [Day]

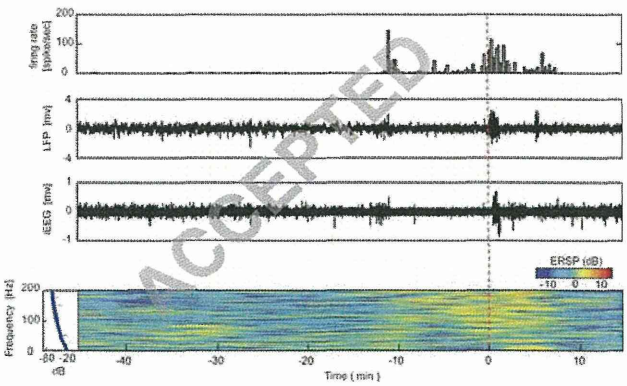
firing rate [spike/sec]
LFP [mv]
iEEG [mv]
ERSP (dB)
Frequency [Hz]
Time (min)

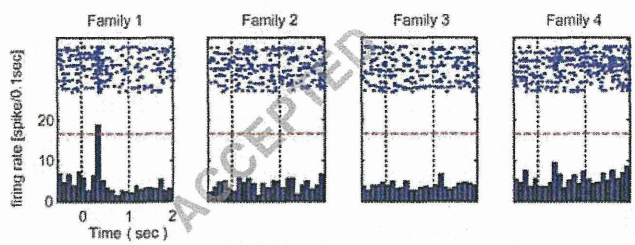
Family 1
Family 2
Family 3
Family 4
firing rate [spike/0.1sec]
Time (sec)

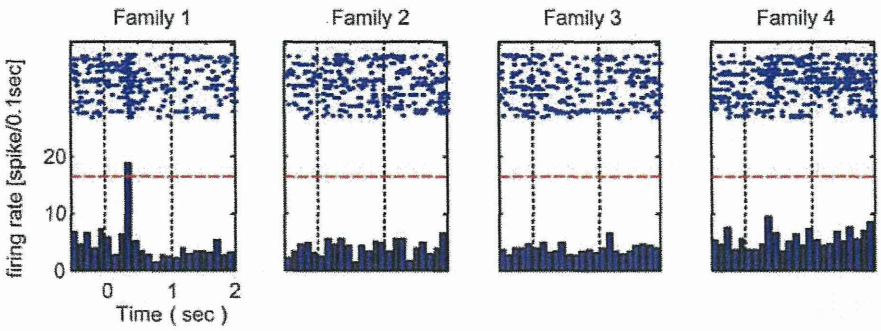

ARTICLE IN PRESS

Brain Stimulation xxx (2012) 1–9

Contents lists available at SciVerse ScienceDirect

Brain Stimulation

journal homepage: www.brainstimjrnl.com

Original Research

Scalp-recorded evoked potentials as a marker for afferent nerve impulse in clinical vagus nerve stimulation

Kenichi Usami [a], Kensuke Kawai [a,*], Masahiro Sonoo [b], Nobuhito Saito [a]

[a] Department of Neurosurgery, Graduate School of Medicine, The University of Tokyo, 7-3-1 Hongo, Bunkyo-ku, Tokyo 113-8655, Japan
[b] Department of Neurology, Teikyo University School of Medicine, Tokyo, Japan

ARTICLE INFO

Article history:
Received 27 April 2012
Received in revised form
19 August 2012
Accepted 18 September 2012
Available online xxx

Keywords:
Epilepsy
Evoked potential
Vagus nerve
Vagus nerve stimulation

ABSTRACT

Background: Vagus nerve stimulation (VNS) is a palliative treatment for drug resistant epilepsy for which the efficacy and safety are well established. Accumulating evidence suggests that ascending vagal signals modulate abnormal cortical excitability via various pathways. However, there is no direct evidence for an ascending conduction of neural impulses in a clinical case of VNS.
Objective: We recorded and analyzed the short-latency components of the vagus nerve (VN) evoked potential (EP) from the viewpoint of determining whether or not it is a marker for the ascending neural conduction.
Methods: EPs within 20 ms were prospectively recorded simultaneously from a surgical wound in the neck and at multiple scalp sites during implantation surgery in 25 patients with drug-resistant epilepsy. Electrical stimulation was delivered using the clinical VNS Therapy system. A recording was made before and after a muscle relaxant was administered, when changing the rostrocaudal position of stimulation, or when stimulating the ansa cervicalis instead of the VN.
Results: The short-latency components consisted of four peaks. The early component around 3 ms, which was most prominent in A1–Cz, remained unchanged after muscle relaxation while the later peaks disappeared. Rostral transition of the stimulation resulted in an earlier shift of the early component. The estimated conduction velocity was 27.4 ± 10.2 m/s. Stimulation of the ansa cervicalis induced no EP.
Conclusions: The early component was regarded as directly resulting from ascending neural conduction of A fibers of the VN, probably originating around the jugular foramen. Recording of VN-EP might document the cause of treatment failure in some patients.

Introduction

Vagus nerve stimulation (VNS) is a widely used adjunctive therapy for drug-resistant epilepsy [1]. Generally VNS reduces the frequency of seizure by approximately 50% in 50% of patients, which shows improvement over time. Independent of its anti-epileptic effects, its antidepressive effects and contribution to cognitive improvement have been suggested as well [2,3]. In contrast to its clinical usefulness and popularity, the underlying mechanisms of action in VNS have not been fully elucidated. In an animal model, VNS induced the expression of c-fos protein in vagus nuclei, the locus coeruleus, cochlear nuclei, the amygdala, the cingulate gyrus, and the retrosplenial cortex, indicating transsynaptic activation of the ascending pathways in the brain [4]. An increase in GABA transmission or a decrease in glutamate transmission in the mediocaudal nucleus of the solitary tract resulted in a reduction of susceptibility to limbic motor seizures [5]. Ascending modulation works on cortical excitability via various ascending pathways including the monoaminergic system [6–8]. Finally, in the cerebral cortex, which is directly associated with epileptogenicity, slow hyperpolarization of pyramidal neurons was induced by VNS [9].

In humans, an enhancement of local inhibition in the primary motor cortex and changes to cerebral blood flow in the thalamus and various regions of cerebral cortices have been observed in association with VNS [10,11]. However, there is no direct evidence

Conflicts of interest: Drs. Usami, Sonoo and Saito report no potential conflicts of interest. Dr. Kawai reports having received lecture fees from Nihon Kohden Corporation.

This work was supported partly by the Ministry of Health, Labour and Welfare of Japan (Grant for Comprehensive Research on Disability, Health and Welfare; H23-Nervous and Muscular-General-003) and partly by Grants-in-Aid for Scientific Research (A) 23240065 and (B) 21390405.

* Corresponding author. Tel.: +81 3 5800 8853; fax: +81 3 5800 8655.
E-mail address: kenkawai-tky@umin.net (K. Kawai).

1935-861X/$ – see front matter © 2012 Elsevier Inc. All rights reserved.
http://dx.doi.org/10.1016/j.brs.2012.09.007

Table 1
Characteristics of patients.

Pt. no.	Sex	Age at seizure onset	Age at start of VNS (yrs)	Diagnosis	Type of seizure	Follow-up duration (month)	Seizure reduction at last follow-up[b] (%)	Antiepileptic drugs
1	M	27 y	30	TLE, postencephalitis	CPS	19	<50	CBZ, PHT, GBP, PHT, LTG
2	M	1 y	13	LGS	GTS, AA, DA	19	<50	VPA, PB, CLB, LTG
3	F	9 m	15	SGE, post West synd.	GTS	19	0	VPA, LTG
4	M	34 y	40	TLE, postencephalitis	CPS, SGTCS	16	>70	PHT, GBP, CLB, VPA, CZP, CLB
5	F	8 m	12	SGE, tuberous sclerosis	CPS	16	<50	VPA, LTG
6	M	23 y	47	TLE	CPS, SGTCS	16	>70	VPA, PHT, CBZ
7	M	2 y	9	FLE, cortical dysplasia	CPS, GTS	16	>70	VPA, CLB, ZNS
8	M	10 y	25	TLE, postencephalitis	CPS, SGTCS	15	<50	LEV, CLB
9	M	25 y	28	TLE, postencephalitis	CPS, SGTCS	13	>50	VPA, PHT, PB, LTG, TPM
10	F	9 m	9	SGE, tuberous sclerosis	SPS, CPS, AA	12	<50	CBZ, TPM, LTG, LEV
11	F	9 y	15	TLE	SPS, CPS, GCS	12	<50	LTG
12	M	7 m	3	SGE, post West synd.	GTS, AA, MS	11	>50	VPA, CZP, ZNS, LTG
13	F	3 y	14	LGS	GTS	11	0	VPA
14	F	31 y	36	FLE	SPS	11	<50	VPA, CBZ, TPM
15	M	1 y	3	CGE	GTS, AA, DA	0[a]	0	PB, ZNS, CZP, LEV
16	M	11 y	13	TLE, postencephalitis	CPS, SGTCS	11	<50	CLB, TPM, LTG
17	M	11 y	32	TLE	SPS, CPS	10	<50	VPA, CBZ, PHT
18	M	3 y	9	TLE	CPS	10	<50	CBZ, CLB, LTG, TPM
19	F	1 y	29	FLE, TLE	CPS, SGTS	9	>50	CBZ, LTG, LEV
20	F	6 y	27	FLE, TLE, HH	CPS, SGTS	9	<50	VPA, CBZ, ZNS, LEV
21	M	15 y	39	TLE	SPS, CPS	9	<50	VPA, PHT, ZNS, CLB, CZP
22	F	12 y	22	FLE, TLE	SPS, CPS	6	>70	PHT, CZP, LTG
23	M	7 y	12	TLE	CPS, SGCS	3	>50	LTG, LEV
24	F	1 y	28	LGS, tuberous sclerosis	GTS	3	<50	CBZ, PHT, LTG
25	M	6 y	18	FLE	GTS	2	>50	VPA, PHT, ZNS, CLB

TLE: temporal lobe epilepsy, LGS: Lennox-Gastaut syndrome, SGE: symptomatic generalized epilepsy, FLE: frontal lobe epilepsy, CGE: cryptogenic generalized epilepsy, HH: hypothalamic hamartoma, CPS: complex partial seizure, GTS: generalized tonic seizure, AA: atypical absence, DA: drop attack, SGTCS: secondary generalized tonic clonic seizure, SPS: simple partial seizure, GCS: generalized clonic seizure, MS: myoclonic seizure, SGTS: secondary generalized tonic seizure, SGCS: secondary generalized clonic seizure, CBZ: carbamazepine, GBP: gabapentine, CLB: clobazam, PHT: phenytoin, LTG: lamotrigine, VPA: valproate, PB: phenobarbital, CZP: clonazepam, ZNS: zonisamide, LEV: levetiracetam, TPM: topiramate.
[a] VNS therapy system was removed 3 weeks after implant surgery due to infection in Patient #15.
[b] Seizure reduction is expressed as % reduction of preoperative frequency.

that ascending conduction of neural impulses is indeed generated by an electrical stimulation of the cervical vagus nerve (VN). Hammond et al. first recorded scalp potentials evoked by clinical VNS [12]. While they observed a large negative peak at around 12 ms following stimulation, it disappeared after administration of a muscle relaxant, indicating that it was an electromyogram of the pharyngeal muscles induced by descending impulses. Tougas et al. described scalp potentials with three peaks of latencies as long as 71 ms, 194 ms and 328 ms [13]. Considering such long latencies, the potentials they observed were regarded as responses induced by polysynaptic neural transmission, not directly reflecting ascending conduction of the VN.

To examine our hypothesis that, in a clinical setting, stimulation of the VN should generate recordable evoked potentials (EPs), such as the early peaks of somatosensory EP and auditory brainstem responses, we prospectively recorded and analyzed the short-latency components of VN-EPs in humans from the viewpoint of whether or not it is a direct marker for the ascending neural conduction.

Materials and methods

Subjects

The subjects of this study were 25 consecutive patients who underwent implantation of the VNS Therapy system (Cyberonics, Houston, TX, USA) for the treatment of drug-resistant epilepsy (Table 1). Board-certified epileptologists made diagnoses of drug-resistant epilepsy and determined an indication for VNS therapy through a routine presurgical evaluation, including long-term video EEG, MRI, ECD-SPECT, IMZ-SPECT, FDG-PET, and neuropsychological assessment. Fifteen of the patients were male and 10 were female. Age distributions were 3–47, median 18 years old. Eleven of them had preceding craniotomy for epilepsy surgery. The number of antiepileptic drugs being administered to those patients at the time of study were 1–6, median 3.0. General and neurological examinations confirmed that none of the patients had systemic and neurological diseases other than epilepsy.

This study was approved by the local ethics committee (The University of Tokyo, Faculty of Medicine; approval number 2592; date of approval June 22, 2009). Written informed consent for this study was obtained from the patients and/or their families.

Recording of VN-EP during VNS implantation

Vagus nerve EP was recorded during implantation surgery of the VNS Therapy system under general anesthesia. The agents used for induction of anesthesia were sodium thiopental in 14 patients, with a mean dosage of 5.1 mg/kg; propofol in 10 patients, with a mean dosage of 2.2 mg/kg; and nitrous oxide in one patient. Muscle relaxants used at the time of anesthetic induction were vecuronium bromide in 22 patients and rocuronium bromide in 3 patients. In all patients, the time between the induction of anesthesia and the start of VN-EP recording was 60–90 min. General anesthesia was maintained with sevoflurane in all patients. Needle electrodes were placed in the patients' scalps at A1, A2, C3, C4, Cz and T5, according to the international 10–20 system. These were connected to a signal processor input box (Neuropack MEB-2200, Nihon Kohden Corporation, Tokyo, Japan). Additionally we placed an A1a electrode on the left

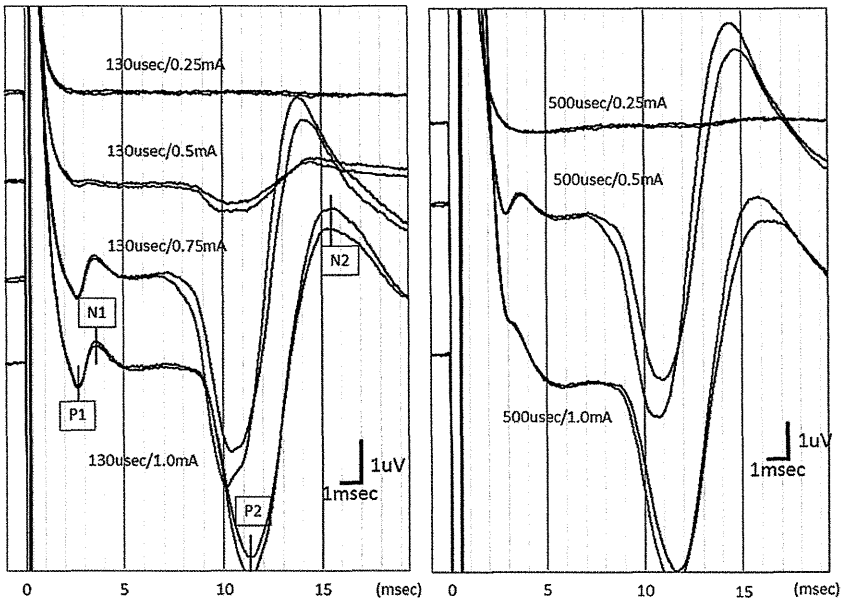

Figure 1. Representative waveforms evoked by various parameters of vagus nerve stimulation. The evoked potentials during 20 ms, beginning 1 ms before each pulse of the VNS, were recorded from scalp electrodes A1–Cz with 50-Hz high-pass, 3000-Hz low-pass, and 50-Hz notch filters, and were averaged for 1000 stimuli. Two representative traces of A1–Cz from a patient are presented. A current of 0.25 mA did not evoke any discernable potential, irrespective of pulse width. As the current and pulse width were increased, small biphasic peaks around 3 ms (P1, N1) immediately following a large stimulation artifact, and large biphasic peaks (P2, N2) around 10 ms, appeared. Further increase in the current and pulse width resulted in an increase of N1 amplitude, but the P1–N1 complex evoked by 500 μs and 1.0 mA was buried in the downslope of the initial stimulation wave and could be recognized only as a tiny notch and a shoulder.

mastoid process and an A1b electrode on the midpoint of A1a and T5. A gelatinous tape electrode (Disposable Earth Electrode, GE Health Care, Tokyo, Japan) was attached circumferentially at the level of the jaw and nape and was connected to the ground to reduce the artifact of stimulation. In 5 patients, an endotracheal tube with electrodes was used for recording of the laryngopharyngeal electromyogram. The tube was equipped with two pairs of bipolar electrodes on each side approximately 4 cm rostral from the tip.

A skin incision was made in the anterior neck approximately 3 cm above the left clavicle. A 3-cm length of the left VN was exposed and completely isolated from the surrounding tissue. The helical electrodes of the VNS Therapy system were coiled around the nerve and connected to the programmable pulse generator. The anchor tether was left unplaced so that we could move the electrodes rostrocaudally along the nerve. After we confirmed with a test-stimulation that there was no adverse event and that the impedance of the electrode was within the expected range, we started stimulation with the VNS Therapy system. We used the magnet mode for stimulation and the parameters were as follows: frequency, 30 Hz; pulse width, 130–750 μs; current, 0.25–2.00 mA; on-time, 60 s. Then we subdermally inserted two needle electrodes to the medial and lateral walls of the surgical wound and connected them to the external trigger of the signal processor.

The montages used for recording were A1–Cz, A2–Cz, C3–Cz, C4–Cz, T5–Cz, A1a–Cz, and A1b–Cz, where Cz was used as a common reference. The signals were amplified and digitized with a sampling rate of 30,000 Hz. The EPs for 20 ms, starting at 1 ms before the external trigger, were recorded with 50-Hz high-pass, 3000-Hz low-pass, and 50-Hz notch filters and were averaged for 1000 recordings. Averaging was started several seconds after the start of stimulation in order to avoid a 2-s ramp-up period, and continued for approximately 33 s (1000 stimuli). The external signal from the needle electrodes close to the VNS helical electrodes in the surgical wound was used as a trigger for averaging.

We recorded the potential at least three times for each condition and for each position of the electrodes. We started each recording several seconds after we turned on the VNS stimulation by placing a magnet over the pulse generator.

In 13 patients, EPs were recorded both before and after the administration of a muscle relaxant. In 3 patients, recording was done without a muscle relaxant. In the remaining 9 patients, recording was done only after a muscle relaxant had been administered. The recording was started 80–100 min after induction of general anesthesia. After we finished the recording of the above-mentioned 13 patients without muscle relaxants, 0.04 mg/kg vecuronium bromide was administered intravenously. After waiting for 2 min, recording of the same patients under muscle relaxation was started.

In some patients, we added the following recordings: First, the helical electrodes of the VNS Therapy system were coiled around the ansa cervicalis and the potentials were recorded before routine recording with stimulation of the VN, for the purpose of investigating whether the potentials were specific for stimulation of the VN ($N = 5$). During surgery, the ansa cervicalis appears over the jugular vein and carotid sheath as we dissect the cervical tissues. Its diameter is thinner than the VN and varies markedly among patients, but it is identifiable in all patients under an operative microscope. Second, the helical electrodes were moved rostrocaudally and measurements were performed at each position, for the purpose of determining whether the conduction is ascending or descending, and to calculate the estimated value of conduction velocity of the VN ($N = 14$). The nerve conduction velocity (NCV) was calculated as follows:

$$NCV = \Delta/(Lc - Lr),$$

where Δ is the distance between the caudal stimulation point and the rostral stimulation point, and Lc and Lr are latencies of the peak of N1 measured at the caudal and rostral stimulation points, respectively. The distance of movement of the helical electrode was visually determined using a tape measure under a surgical microscope (Supplement 1). Furthermore, additional recordings were done while moving the trigger electrodes from within the wound to 5 cm outside of the wound, changing the distance between the trigger electrodes and the helical electrodes of VNS, for the purpose of confirming the stability and reliability of the trigger electrodes ($N = 1$).

The total recording time was less than 1 h in all patients. After all measurements had been completed, we placed the pulse generator in a subcutaneous pocket of the left anterior chest and closed the wound. There were no adverse events associated with this study.

Data analysis

The EPs were saved as image data of acquired traces and as numerical data with a timeline in all patients. Two traces out of three were selected from the viewpoint of stability and consistency by visually inspecting the traces.

First, we determined the latency of peaks in waveforms using a cursor of the signal processor by visual inspection. The processor began timing from zero at the moment of the external trigger. An average value of the two traces was used. In those patients in whom more than one recording was done due to changing the position of stimulation, we used an averaged value of those recordings to present the rough latency of the P1–N1 complex, because the final electrode position at the end of implantation surgery was approximately at the midpoint of two stimulation positions.

In some patients, early peaks were buried in the downslope of the initial stimulation wave and were identified only as a tiny notch and a shoulder, so it was difficult to exactly determine the latency of the peaks (see Fig. 1). Therefore, secondly, we determined their latencies in the estimated waveform after elimination of the initial stimulation wave. Curve fitting to an exponential function was applied to the range between 0.8–1.8 ms of the original numerical data using Microsoft Excel. Then we extracted the evoked component by subtracting the approximated value from the original value at each time point (Supplement 2):

$$Pi = Oi - \exp(Ti),$$

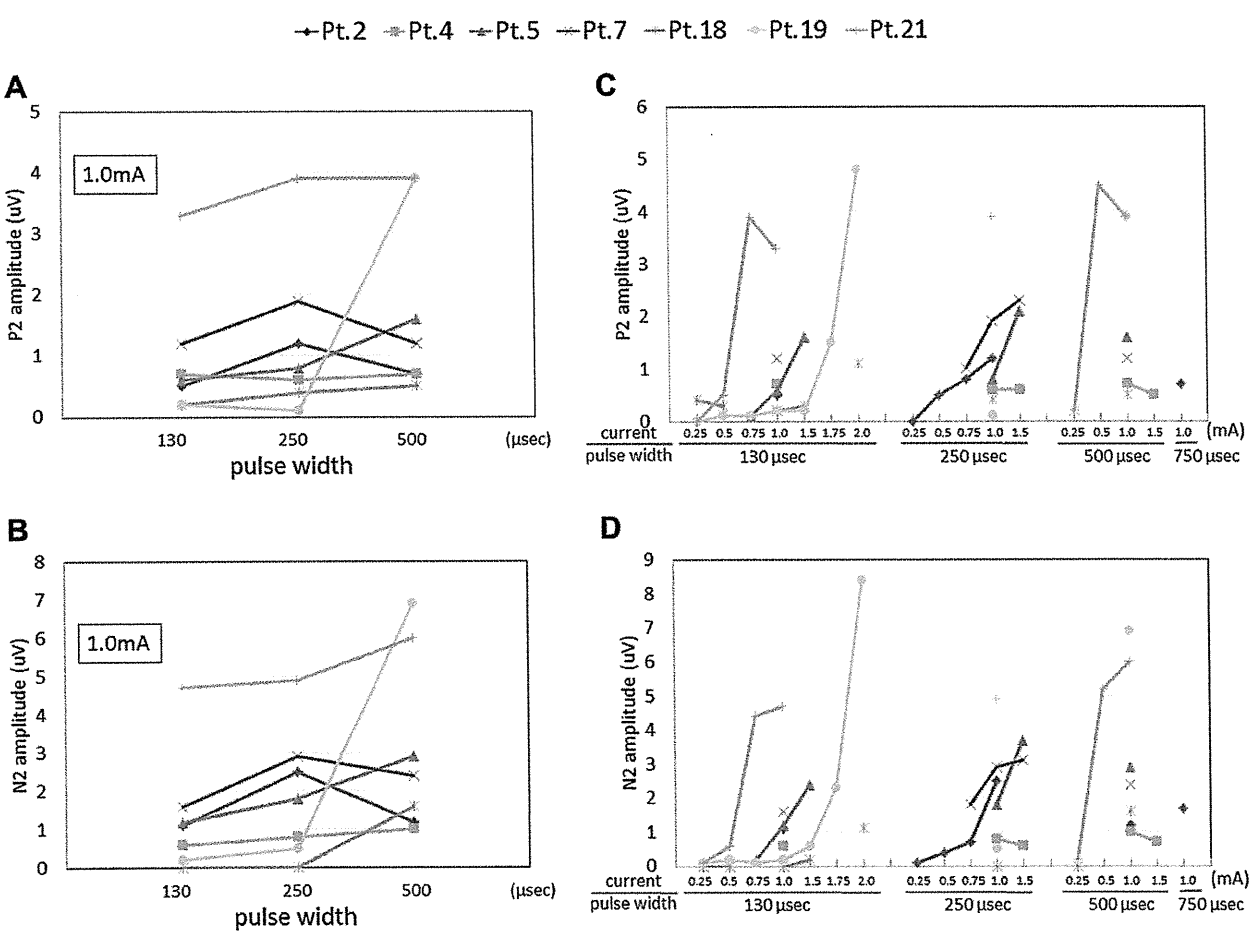

Figure 2. Association between the P2 and N2 amplitudes and the VNS parameters in each patient ($n = 7$). Each line represents a patient. (A) and (B) demonstrate the amplitudes of P2 and N2, respectively, when stimulated with three pulse widths at a fixed current of 1.0 mA. The pulse width did not seem to significantly affect the amplitudes of P2 and N2 in all patients except one (Patient # 19). (C) and (D) demonstrate the amplitudes of P2 and N2, respectively, when stimulated with various currents. The current seemed to affect the amplitudes in a sigmoid fashion.

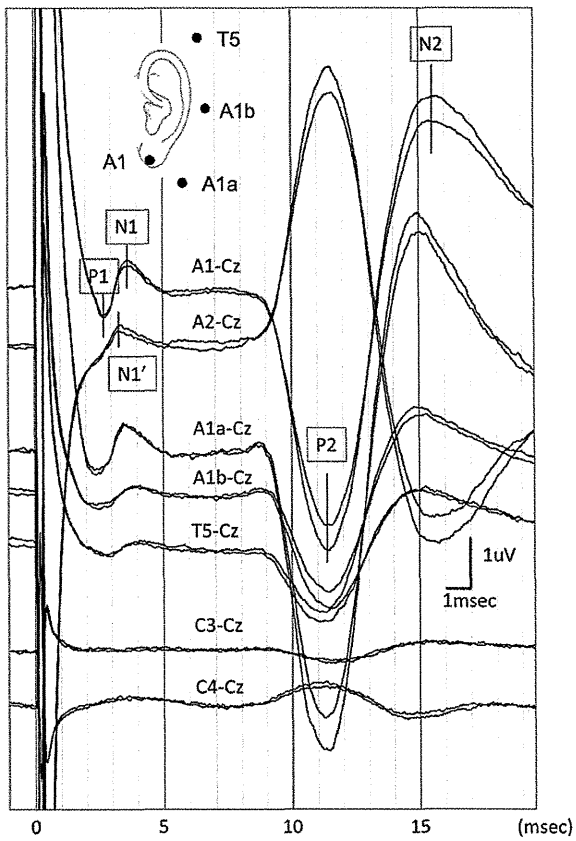

Figure 3. Vagus nerve evoked potentials recorded in different montages. Two traces from a single patient without muscle relaxation. The parameters of VNS were a current of 1.0 mA, a pulse width of 130 μs, and a frequency of 30 Hz. The early negative peak (N1) was most prominent in montages A1–Cz and A1a–Cz. It gradually decreased its amplitude as the exploring electrodes separated away from the skullbase from A1a to A1b to T5. A smaller negative peak (N1′) was noted in A2–Cz slightly earlier than the N1 observed in A1–Cz. Large peaks (P2, N2) of the late component showed a phase reversal between the sides of exploring electrodes.

where *Pi* is the estimated evoked component at time point *i*, *Oi* is the original value of potential at time point *i*, and *Ti* is the time at *i*. Using the thus extracted data, we determined the latency and amplitude of early peaks. The signal processor saved the original data, starting 1 ms before the trigger point. Time zero was defined as the time point where a huge (>1 μV) abrupt change of amplitude occurred for around 1 ms. The baseline amplitude was defined as the mean amplitude of the first 1 ms. The amplitude of the early component was defined as the difference between the amplitudes of positive and negative peaks. The appropriateness of approximation with an exponential function was confirmed in the data where no early components were evoked, i.e., stimulation of the ansa cervicalis and stimulation with minimal parameters, that is, 0.25 mA and 130 μs.

To assess the effect of stimulation parameters on the amplitudes of the early and late components, we drew input–output curves. The amplitude of P2 and N2 were determined as the absolute difference from baseline. Determination of the amplitude of the P1–N1 complex has been described above. In 4 patients (#16, #17, #18, #19), whose recordings were done with caudal and rostral stimulations, measurements with various parameters were done only during caudal stimulation.

The values were presented as mean ± standard deviation among patients.

Results

Waveform of VN-EP

The waveforms evoked by clinical VNS were highly reproducible within each patient and consistent among the patients. The initial stimulation wave was a huge wave consisting of a momentary biphasic spike and a subsequent exponential downslope in all patients. Following the initial stimulation wave, we typically observed four peaks in the waveform (Fig. 1). The early and late peaks were with a latency shorter and longer than 5 ms, respectively. We named the early smaller positive and negative peaks as P1 and N1, respectively, and the subsequent larger positive and negative peaks as P2 and N2, respectively.

The P1–N1 complex was recognizable in all patients except two, in whom no waveform was observed in one (Patient #20) and only a late component in the other (Patient #3). In Patient #20, various parameters of stimulation were applied but no potentials other than the initial stimulation wave were generated. In Patient #3, a pulse width of only 500 μs was used. In patients in whom visual determination of N1 was possible ($N = 23$), its latency in A1–Cz was 3.3 ± 0.4 ms (range 2.5–4.2).

The P2–N2 complex consisted of a large positive peak (P2) at 6.4–11.1 ms and a subsequent large negative peak (N2) at 9.2–15.1 ms when the exploring electrode was on the left side. The P2–N2 complex was identified in all patients in whom recording was done without muscle relaxants except two, in whom no waveform was observed in one (#20) and only an early component in the other (#17).

Effect of stimulation parameters

Minimal stimulation of the VN with 0.25 mA and 130 μs did not induce the early and late complexes but did reproducibly induce the initial stimulation wave (Fig. 1). When the pulse width and/or current were increased, it seemed that the amplitude of the P1–N1 complex increased but the latency did not. The downslope of the initial stimulation wave was prolonged as well. A further increase to 500 μs and 1.0 mA resulted in a paradoxical decrease of the P1–N1 complex, so that it was only identifiable as a tiny notch and a shoulder in the downslope. Therefore, the amplitude of the P1–N1 complex, as determined by visual inspection, did not reflect the genuine amplitude of the EP. We measured the P1–N1 amplitude in the estimated waveform after elimination of the initial stimulation wave, which is presented below.

The association between the P2 and N2 amplitudes and the VNS parameters in each patient is presented in Fig. 2. The pulse width did not seem to significantly affect the amplitudes of P2 and N2, whereas the current did seem to affect their amplitudes in a sigmoid fashion.

Topographical distribution of EP

The P1–N1 and P2–N2 complexes were most prominent in montages A1–Cz and A1a–Cz (Fig. 3). They gradually decreased as the exploring electrodes separated away from the skullbase, from A1a to A1b to T5. In A2–Cz, the phase of the initial stimulation wave and the P2–N2 complex were reversed, but the phase of the early complex (N1′) was not reversed. The latency of the N1′ peak in A2–Cz was slightly earlier than the N1 peak in A1–Cz. The waveform of the P2–N2 complex was not only reversed but almost completely symmetrical in A1–Cz and A2–Cz. The P2–N2 complex was discernable in C3–Cz and C4–Cz as a smaller similarity of

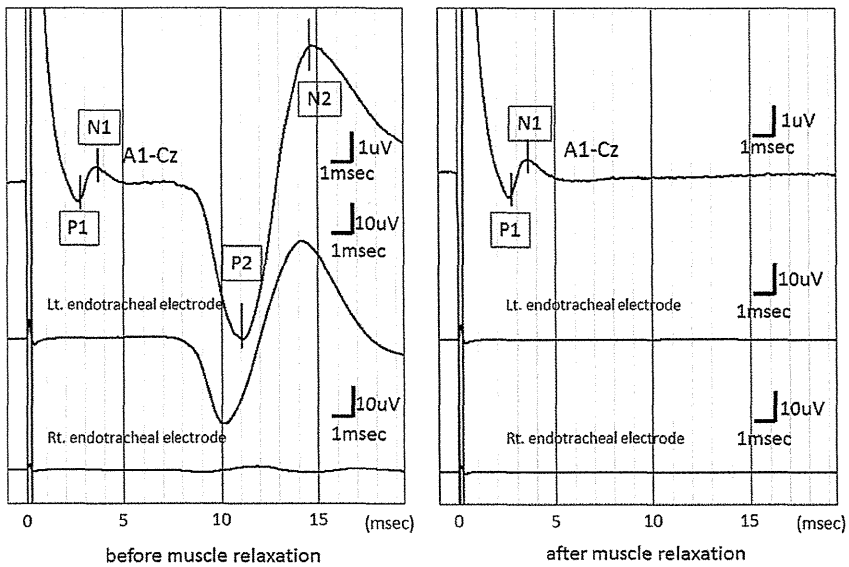

Figure 4. Vagus nerve evoked potential, endotracheal electromyogram (EMG), and effect of muscle relaxation. The endotracheal EMG was recorded dominantly from the left side. Its waveform was a much larger and slightly earlier similarity of the late components in A1–Cz. Note the scale is different between the top trace and the lower two traces. After administration of a muscle relaxant, the endotracheal EMG and the late component in A1–Cz disappeared, while the early component was unchanged. Representative traces from a patient are presented.

A1–Cz and A2–Cz, respectively, but the P1–N1 complex was not discernable in C3–Cz and C4–Cz.

Effect of muscle relaxation

Under muscle relaxation, the initial stimulation wave and the P1–N1 complex remained unchanged, while the P2–N2 complex completely disappeared (Fig. 4). The disappearance of the late components and preservation of the early component under muscle relaxation were observed in all of the 13 patients in whom both of the components were detected before muscle relaxation. Simultaneous recording from the endotracheal electrodes demonstrated no early component but rather a late component similar to the P2–N2 complex in A1–Cz. This was more prominent on the left side and its waveform was a much larger similarity of the P2–N2 complex. The phases were identical but the peaks were approximately 1 ms earlier in the endotracheal electrodes. The potential in the endotracheal electrode completely disappeared under muscle relaxation.

Stimulation of ansa cervicalis

Stimulation of the ansa cervicalis resulted in a consistent and reproducible stimulation wave, but no other discernable potentials were evoked including the P1–N1 and P2–N2 complexes (Fig. 5).

Effect of stimulating position

Evoked potentials were recorded while changing the rostrocaudal position of helical stimulation electrodes along the VN

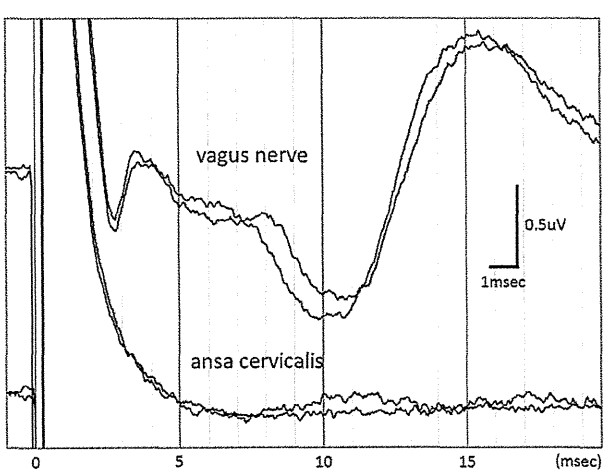

Figure 5. No potential was evoked when the ansa cervicalis was stimulated. Representative traces are presented from a single patient. Stimulation parameters were a current of 1.0 mA, a frequency of 30 Hz, and a pulse width of 130 μs.

Table 2
Distance of electrode movement, visually determined latency of N1, and estimated value of nerve conduction velocity.

Patient #	Δ (mm)	Lc (ms)	Lr (ms)	Lr-Lc (ms)	NCV (m/s)
8	12	3.1	3.5	−0.3	N/A
9	12	3.7	3.1	0.6	19.4
10	8	3.6	3.3	0.3	25.8
11	6	3.2	3.6	−0.3	N/A
12	5	3.0	2.3	0.7	6.8
14	11	3.0	2.7	0.3	32.4
16	10	4.0	3.8	0.2	41.7
17	7.5	3.6	3.4	0.2	37.5
18	9	2.9	2.6	0.3	30.0
19	14	2.7	2.2	0.5	28.0
22	10	3.0	2.6	0.4	25.0
23	12	3.1	V/U		N/A
24	8	2.9	3.2	−0.3	N/A
25	9	3.7	V/U		N/A
Mean	9.5	3.3	3.0	0.4	27.4
SD	2.5	0.4	0.5	0.2	10.2

Δ, distance (mm) of transition from the caudal stimulating point to the rostral stimulating point. Lc (ms), latency of N1 measured with caudal stimulation. Lr (ms), latency of N1 measured with rostral stimulation. NCV (m/s), nerve conduction velocity, calculated as Δ/(Lc−Lr). V/U, visually undetermined. SD, standard deviation.

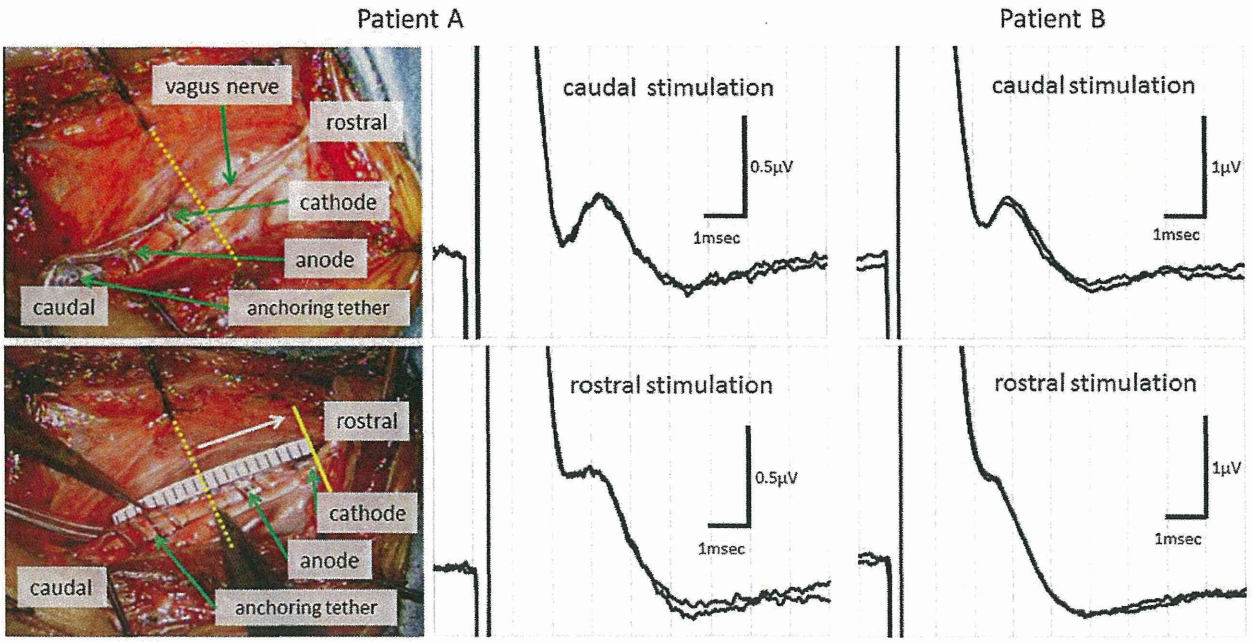

Figure 6. Effect of stimulation position. Evoked potentials were recorded while changing the rostrocaudal position of the helical stimulation electrode along the vagus nerve. In this patient (Patient #14 in Table 1), the rostral end of the cathode was moved from the yellow dotted line to the yellow solid line. The movement was 11 mm. Representative recordings in 2 patients are presented. In Patient A (Patient #14 in Table 1), an earlier shift of the P1–N1 complex by rostral transition of stimulation is clearly discernable. In Patient B (Patient #23 in Table 1), the earlier shift is not very clear.

in 14 patients. The distance of movement was 9.5 ± 2.5 mm (Table 2). With the rostral movement of the stimulation electrodes, an earlier shift of the P1–N1 complex was observed by visual inspection in 11 patients (Fig. 6). In the remaining 3 patients, there was no recognizable latency shift by visual inspection. In 9 patients in whom N1 latencies in both rostral and caudal stimulation could be determined by visual inspection, the estimated nerve conduction velocity was 27.4 ± 10.2 m/s (Table 2).

Extraction of P1–N1 complex and estimation of nerve conduction velocity

An exponential curve estimated from the initial 0.8–1.8 ms was well fit to the subsequent 1.8–5.0 ms of the original data where the ansa cervicalis was stimulated ($N = 5$, correlation coefficient 0.967) and the stimulation parameters were minimal ($N = 4$, correlation coefficient 0.942). We regarded the approximation method as acceptable and used it as another determination method of P1–N1 complex latencies and amplitude, instead of visual determination.

Using this approximation and extraction of the waveform, the P1–N1 complex became clearer so that the peaks could be determined ($N = 14$). Table 3 is a summary of the latencies thus determined in all patients. The latencies of P1 and N1 were 2.5 ± 0.3 ms and 3.6 ± 0.5 ms, respectively, which were consistent with the values determined by visual inspection in 11 patients. The estimated nerve conduction velocity, calculated from a shift of N1 latency and the distance of stimulation points, was 30.4 ± 15.4 m/s. Fig. 7 demonstrates the association of the P1–N1 complex amplitude with stimulation parameters. In 7 of 9 patients, an increase in the stimulation current resulted in an associated increase in amplitude. The pulse width did not affect the amplitude.

Effect of position of trigger electrodes

Moving the trigger-electrode from within the surgical wound to 5 cm outside of the wound did not cause any changes in the waveform and latencies of the EP.

Discussion

A previous study by Hammond et al. demonstrated that the late component of VN-EP had been recorded in a clinical setting [12]. They suggested that the EP was a laryngopharyngeal electromyogram because it disappeared after the administration of a muscle

Table 3
Latencies of P1 and N1 determined by curve fitting, and estimated nerve conduction velocity.

Patient #	Δ (mm)	Latency of P1 (ms)			Latency of N1 (ms)			NCV (m/s)
		Distal	Proximal	Mean	Distal	Proximal	Mean	
8	12	2.6	3.1	2.9	3.8	4.2	4.0	N/A
9	12	2.9	2.5	2.7	4.1	3.5	3.8	21.6
10	8	2.6	2.5	2.6	3.9	3.7	3.8	28.1
11	6	2.5	2.4	2.5	4.0	3.8	3.9	37.5
12	5	2.4	1.8	2.1	3.7	3.0	3.4	7.6
14	11	2.4	2.2	2.3	3.6	3.3	3.4	31.0
16	10	3.1	2.9	3.0	4.6	4.6	4.6	N/A
17	7.5	2.9	2.7	2.8	4.0	3.8	3.9	26.8
18	9	2.3	2.2	2.3	3.1	2.7	2.9	25.4
19	14	2.5	1.9	2.2	3.3	2.8	3.1	34.1
22	10	2.5	2.3	2.4	3.6	3.2	3.4	23.8
23	12	2.4	2.0	2.2	3.4	3.1	3.2	33.3
24	8	2.2	2.1	2.2	3.2	3.1	3.2	72.7
25	9	2.8	2.7	2.7	3.8	3.5	3.7	23.1
Mean	9.5			2.5			3.6	30.4
SD	2.5			0.3			0.5	15.4

Δ, distance (mm) of transition from the caudal stimulating point to the rostral stimulating point. NCV (m/s), nerve conduction velocity, calculated from shift of N1 latency and Δ. SD, standard deviation.

relaxant. We observed the same EP component, but for the first time identified the early component, which did not disappear under muscle relaxation. The early component P1–N1 complex shifted earlier when the stimulation electrodes were moved rostrally. It was specific to vagal stimulation because stimulation of the ansa cervicalis, very close to the VN, did not induce any EP. Therefore, it was highly probable that the P1–N1 we observed was direct evidence of the afferent conduction of the VN in humans.

The reason why previous researchers were unable to recognize the early EP component is unclear [12,13]. But they seemed to focus on long-latency potentials from the outset of their studies. As we demonstrated here, the early component was easily buried in the initial stimulation wave. To detect the early component constantly, stimulation with shorter pulse widths was preferable. Larger currents and larger pulse widths made the P1–N1 complex less discernable due to the larger initial stimulation wave.

As for the origin of the early component, we observed the largest waveform from the auricle and the mastoid process. Therefore, it was considered to originate from around the brainstem, skullbase, or the upper cervical region. We can estimate the distance between the stimulation point and the generator of EP by multiplying the calculated value of NCV (27 m/s) by the measured value of the N1 latency (3.3 ms). It is estimated to be 89.1 mm, consistent with the distance between the surgical wound in the neck and the skullbase.

The main sources of EPs are axonal-conducting action potentials and postsynaptic potentials. A junctional potential is generated by a change in the size or impedance of the volume conductor around the nerve, by a directional change of the nerve course, or at the beginning or end of the nerve conduction [14]. The VN passes through the jugular foramen and connects to multiple nuclei, including the spinal tract nucleus, the medial reticular formation of the medulla, the area postrema, the dorsal nucleus of the VN, the ambiguous nucleus, and the solitary tract nucleus [15]. Applying the above-mentioned rule to the VN, we can speculate that the early component was most likely generated at the entrance into the cranium, the jugular foramen, where the impedance around the nerve changes. Contributions of the terminal potentials and post-synaptic potentials in the medulla oblongata are considered less likely since the VN disperses to multiple nuclei within it. The above theory of junctional potential may also explain why the N1′ potential recorded in the A2–Cz lead had an earlier peak than the N1 recorded in the A1–Cz lead. Viewing from the A2 electrode position, the ascending impulse along the VN hides itself behind the massive cranial bone and vertebra, before its true entrance into the

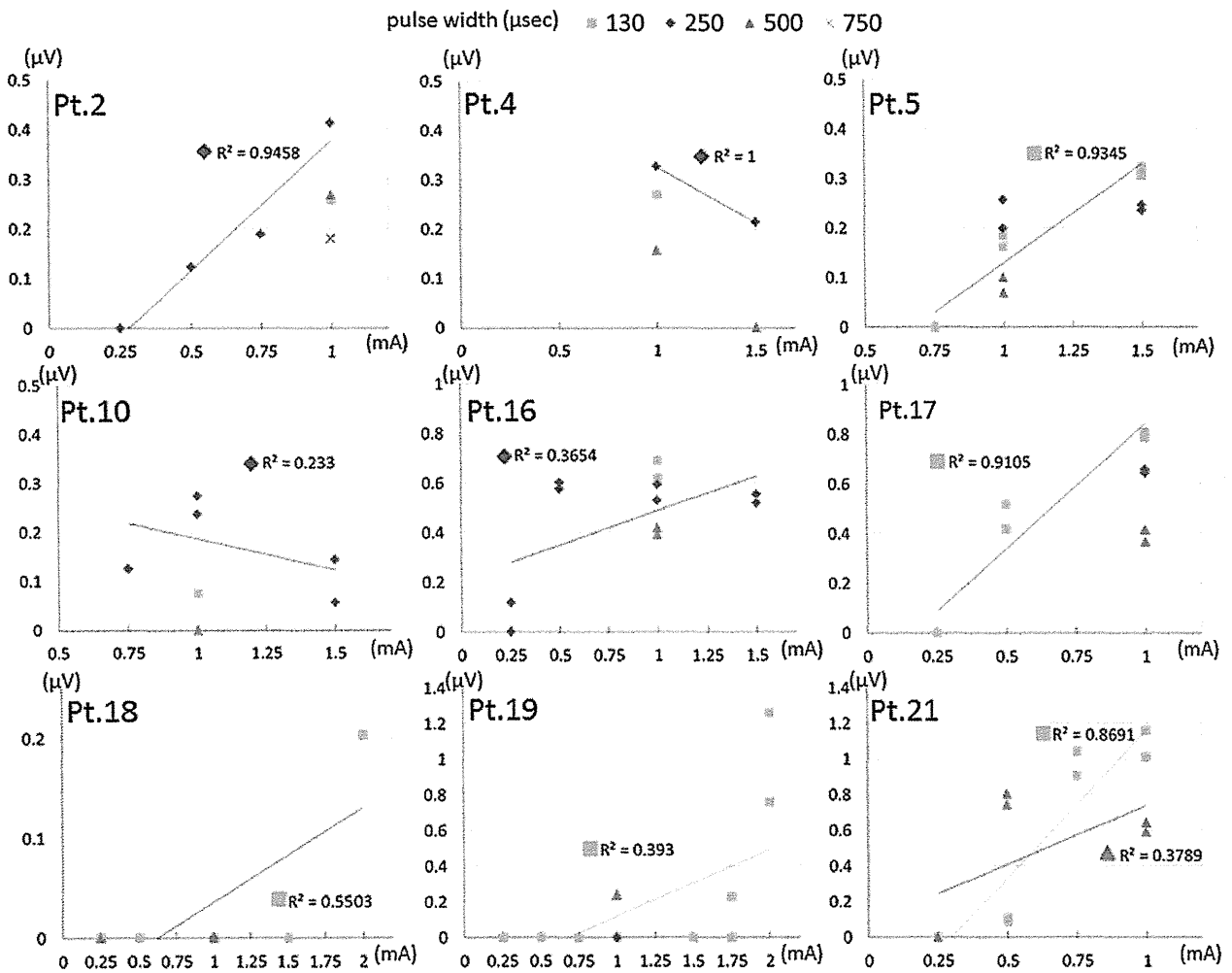

Figure 7. Association between the amplitude of P1–N1 complex and the VNS parameters in 9 patients. Horizontal and vertical axes represent the current and the estimated amplitude of the P1–N1 complex, respectively. For estimation of the amplitude of the P1–N1 complex, see the 'Data analysis' section of the text. Each regression line represents the association of current and amplitude to a fixed value of pulse width. R^2 is the correlation coefficient. In Patient 21, two regression lines are shown because we recorded with multiple currents to pulse widths of 130 μs (—) and 500 μs (—). In 7 of 9 patients, an increase in stimulation current resulted in an associated increase in the amplitude, while the pulse width did not affect the amplitude.

skullbase. Therefore, the junctional potential may be generated slightly earlier than the N1 potential.

As for the late component, we postulated that the P2–N2 complex was the same potential as that observed in a previous study [12]. It is highly probable that the P2–N2 complex reflects the laryngopharyngeal electromyogram, since it disappeared after the administration of a muscle relaxant and its waveform was similar to that in endotracheal electrodes. The finding that their latencies were slightly later than those in the laryngopharyngeal electrodes and that their waveforms were almost symmetrical in A1–Cz and A2–Cz suggests that the generator was located far away and in the center, supporting the laryngopharyngeal electromyogram notion.

Eighty percent of the VN at the cervical portion is afferent fiber [16], which consists of 3 components, Aβ, Aγ and C fibers [17,18]. The conduction velocity of Aβ fibers is the fastest and that of C fibers is the slowest. The threshold producing an action potential is the lowest in Aβ fibers and the highest in C fibers. Previous studies suggested that the neural conduction of A fibers contributes to antiepileptic effects [9,18,19]. The estimated nerve conduction velocity was 27.4 ± 10.2 m/s in our study, which fell in the range of A fibers and was consistent with previous studies.

This study was the first to demonstrate in a clinical setting that VNS in humans generates ascending afferent nerve conduction, revealing some aspects of electrophysiological properties of the human VN. We did not directly prove the clinical usefulness for the recording of VN-EP, but we assume its significance in two aspects: First, it can be used to confirm the VN intraoperatively; in some patients, the ansa cervicalis is very thick and for inexperienced surgeons there may be a risk of misjudgment, particularly when the implantation surgery is done with a very small surgical wound. Second, the recording of VN-EP may explain the cause of treatment failure in some patients and might predict the outcome of treatment. For that purpose, further research is needed to study the association of VN-EP properties and the efficacy of VNS in epilepsy patients.

Acknowledgments

The authors thank Mr. Hitoshi Sano of Nihon Kohden Corporation for his technical and theoretical support.

Supplementary data

Supplementary data related to this article can be found online at http://dx.doi.org/10.1016/j.brs.2012.09.007

References

[1] Ben-Menachem E. Vagus-nerve stimulation for the treatment of epilepsy. Lancet Neurology 2002;1(8):477–82.
[2] Clark KB, Naritoku DK, Smith DC, Browning RA, Jensen RA. Enhanced recognition memory following vagus nerve stimulation in human subjects. Nature Neuroscience 1999;2(1):94–8.
[3] Elger G, Hoppe C, Falkai P, Rush AJ, Elger CE. Vagus nerve stimulation is associated with mood improvements in epilepsy patients. Epilepsy Research 2000;42(2-3):203–10.
[4] Naritoku DK, Terry WJ, Helfert RH. Regional induction of fos immunoreactivity in the brain by anticonvulsant stimulation of the vagus nerve. Epilepsy Research 1995;22(1):53–62.
[5] Walker BR, Easton A, Gale K. Regulation of limbic motor seizures by GABA and glutamate transmission in nucleus tractus solitarius. Epilepsia 1999;40(8): 1051–7.
[6] Krahl SE, Clark KB, Smith DC, Browning RA. Locus coeruleus lesions suppress the seizure-attenuating effects of vagus nerve stimulation. Epilepsia 1998; 39(7):709–14.
[7] Groves DA, Bowman EM, Brown VJ. Recordings from the rat locus coeruleus during acute vagal nerve stimulation in the anaesthetised rat. Neuroscience Letters 2005;379(3):174–9.
[8] Manta S, Dong J, Debonnel G, Blier P. Enhancement of the function of rat serotonin and norepinephrine neurons by sustained vagus nerve stimulation. Journal of Psychiatry & Neuroscience 2009;34(4):272–80.
[9] Zagon A, Kemeny AA. Slow hyperpolarization in cortical neurons: a possible mechanism behind vagus nerve simulation therapy for refractory epilepsy? Epilepsia 2000;41(11):1382–9.
[10] Henry TR, Votaw JR, Pennell PB, Epstein CM, Bakay RA, Faber TL, et al. Acute blood flow changes and efficacy of vagus nerve stimulation in partial epilepsy. Neurology 1999;52(6):1166–73.
[11] Di Lazzaro V, Oliviero A, Pilato F, Saturno E, Dileone M, Meglio M, et al. Effects of vagus nerve stimulation on cortical excitability in epileptic patients. Neurology 2004;62(12):2310–2.
[12] Hammond EJ, Uthman BM, Reid SA, Wilder BJ. Electrophysiologic studies of cervical vagus nerve stimulation in humans: II. Evoked potentials. Epilepsia 1992;33(6):1021–8.
[13] Tougas G, Hudoba P, Fitzpatrick D, Hunt RH, Upton AR. Cerebral-evoked potential responses following direct vagal and esophageal electrical stimulation in humans. American Journal of Physiology 1993;264(3 Pt 1): G486–91.
[14] Sonoo M. How much has been solved regarding SEP generators? Electroencephalography and Clinical Neurophysiology. Supplement 1999;49: 47–51.
[15] Henry TR. Therapeutic mechanisms of vagus nerve stimulation. Neurology 2002;59(6 Suppl. 4):S3–14.
[16] Foley JO, DuBois FS. Quantitative studies of the vagus nerve in the cat. I. The ratio of sensory to motor fibers. Journal of Comparative Neurology 1937;67: 49–67.
[17] Li CL, Mathews G, Bak AF. Action potential of somatic and autonomic nerves. Experimental Neurology 1977;56(3):527–37.
[18] Evans MS, Verma-Ahuja S, Naritoku DK, Espinosa JA. Intraoperative human vagus nerve compound action potentials. Acta Neurologica Scandinavica 2004;110(4):232–8.
[19] Krahl SE, Senanayake SS, Handforth A. Destruction of peripheral C-fibers does not alter subsequent vagus nerve stimulation-induced seizure suppression in rats. Epilepsia 2001;42(5):586–9.

ELSEVIER

Brain & Development xxx (2013) xxx–xxx

BRAIN & DEVELOPMENT
Official Journal of the Japanese Society of Child Neurology

www.elsevier.com/locate/braindev

Original article

Modification of vertical hemispherotomy for refractory epilepsy ☆

Kensuke Kawai [a,*], Michiharu Morino [b], Masaki Iwasaki [c]

[a] *Department of Neurosurgery, The University of Tokyo, Japan*
[b] *Department of Neurosurgery, Tokyo Metropolitan Neurological Hospital, Japan*
[c] *Department of Neurosurgery, Tohoku University, Japan*

Received 12 November 2012; received in revised form 28 December 2012; accepted 30 December 2012

Abstract

Delalande's vertical hemispherotomy is an innovative evolution of hemispherectomy in minimizing brain resection. We report our modification for this surgical procedure. We modified the original procedure in two aspects for the purpose of less brain resection and confirmation of the complete disconnection. Firstly, all procedures were done via an interhemispheric route instead of a transcortical route. Secondly, we set the anterior disconnection plane as the one that connects the anterior end of the choroidal fissure to the anterior end of the foramen of Monro, instead of the former to the subcallosal area. We applied this modified vertical hemispherotomy to 7 cases. Four cases were children with hemimegalencephaly and other 3 were adults with ulegyric hemisphere. Surgical procedure was completed without complication in all cases. There was no case that required CSF shunting. Seizure outcome was Engel's class I in 6 and class IV in 1. Postoperative MRI revealed complete disconnection of the affected hemisphere in all patients. We reported our modification of vertical hemispherotomy. Although these are minor modifications, they further minimized brain resection and may serve for less invasiveness of procedure and improvement in completeness of disconnection and its confirmation during surgery.

Keywords: Epilepsy; Epilepsy surgery; Hemispherectomy; Hemispherotomy

1. Introduction

Hemispherectomy is the most effective surgical treatment for hemispheric epilepsy. Surgical procedure of hemispherectomy has been developed over the past decades. Functional hemispherectomy by Rasmussen was the first to introduce the concept of disconnection of epileptic cortices [1]. Thereafter, several surgeons modified the procedure to further reduce the volume of brain resection by making the disconnection of the white matter tracts as the major procedure instead of resection [2–5]. These modified functional hemispherectomies are called hemispherotomy. While the most procedures of hemispherotomy used a lateral approach to the brain according to Rasmussen's original functional hemispherectomy [3–5], Delalande first proposed a novel hemispherotomy procedure in 1990s [6]. It was innovative in using a vertical approach and achieving the complete disconnection of affected cortices with much less volume of brain resection than the lateral approaches.

One of the authors reviewed the hemispherotomy series at Tokyo Metropolitan Neurological Hospital [7]. In this study, the procedure was reviewed by decomposing into a disconnection of the commissural fibers and a disconnection of the projection fibers, and the elemental surgical procedures were compared in terms of the completeness of disconnection and the occurrence of complication. The major findings were that interhemispheric

☆ Part of this work has been presented at the International Symposium on Surgery for Catastrophic Epilepsy in Infants (ISCE), the Fourteenth Annual Meeting of ISS, Tokyo, February 18-19, 2012.

* Corresponding author. Address: Department of Neurosurgery, Graduate School of Medicine, The University of Tokyo, 7-3-1 Hongo, Bunkyo, Tokyo 113-8655, Japan. Tel.: +81 3 5800 8853; fax: +81 3 5800 8655.
E-mail address: kenkawai-tky@umin.net (K. Kawai).

0387-7604/$ - see front matter © 2013 Published by Elsevier B.V. on behalf of The Japanese Society of Child Neurology.
http://dx.doi.org/10.1016/j.braindev.2012.12.013

Please cite this article in press as: Kawai K et al. Modification of vertical hemispherotomy for refractory epilepsy. Brain Dev (2013), http://dx.doi.org/10.1016/j.braindev.2012.12.013

Table 1
Clinical information of 7 patients.

Patient	Age at onset of seizure	Type of seizure	Frequency of seizure	Preoperative AED[a]	MRIfindings/ etiology	Distribution of epileptiform abnormality in EEG	Others	Preoperative IQ, DQ or neurological state	Age at surgery	Side of surgery	Follow up (years)	Seizure outcome[b]
1	1 day	GCS	Multiple daily	PB(20) VPA(150) MDZ(0.05)	Lt. hemimegalencephaly	Lt. hemispheric	rCBF-SPECT: rt. hemispheric increase	Hypotonic, minimal extremities movement	2 months	Left	9	I
2	5 years	CPS, HC	Weekly	PHT(300) VPA(1200) CBZ(900) CZP(2)	Rt. hemiatrophy, porencephaly/ cerebral palsy	Rt. hemispheric	FDG-PET: rt. hemispheric decrease	VIQ 60 PIQ 47 FIQ 49	40 years	Right	8	I
3	9 years	MS, TS	Monthly	VPA(1200) CBZ(700) CLB(10)	Lt. diffuse ulegyria/ posttraumatic	Lt. hemispheric	FDG-PET: lt. hemispheric decrease	VIQ 54 PIQ so FIQ 40	21 years	Left	7	I
4	1 day	CPS, HC, TS	Multiple daily	PB(32) ZNS(60) CLB(3.2)	Rt. hemimegalencephaly	Bilateral, diffuse	FDG-PET: rt. temporal decrease	Not tested but delay in milestone	4 months	Right	5	I
5	1 day	GCS HC	Multiple daily	PHT(150) CBZ(400) MDZ(0.3)	Lt. hemimegalencephaly	Lt. hemispheric	FDG-PET: lt. hemispheric decrease	Not tested	6 months	Left	4	I
6	1 day	TS	Multiple daily	PB(100) CBZ(160) PHT(115)	Rt. hemimegalencephaly	Bilateral, diffuse	FDG-PET: rt. hemispheric and left frontal decrease	Not tested	7 months	Right	4	IV
7	1 year	CPS	Multiple daily	CBZ(900) VPA(1200)	Lt. hemiatrophy/ postvaccination	Lt. hemispheric	FDG-PET: rt. hemispheric decrease	VIQ 62 PIQ 49 FIQ 51	41 years	Left	0.5	I

AED, antiepileptic drug; CPS, complex partial seizure; GCS, generalized convulsive seizure; HC, hemiconvulsion; lt., left; MDZ, midazolam; MS, myoclonic seizure; PB, phenobarbital; rt., right; so, scale out; TS, tonic seizure; VPA, valproic acid.

[a] Dose is shown in parenthesis (mg). Midazolam was administered intravenous continuously (mg/kg/h).

[b] Engel's classification. Class I means free of disabling seizures since surgery. Class IV means no worthwhile improvement.

Please cite this article in press as: Kawai K et al. Modification of vertical hemispherotomy for refractory epilepsy. Brain Dev (2013), http://dx.doi.org/10.1016/j.braindev.2012.12.013

callosotomy was securer than transventricular callosotomy, and that the less brain resection results in the less complication associated with circulation of the cerebrospinal fluid. Based on these findings, we adopted Delalande's vertical hemispherotomy because it used vertical callosotomy that is similar to interhemispheric callosotomy and resected only a small volume of the brain. We further made minor modifications to the original vertical hemispherotomy by using the interhemispheric callosotomy and further reducing the volume of brain resection, which we present in this report.

2. Methods

2.1. Patients

We adopted the modified hemispherotomy to 7 patients. Four patients underwent surgery by one of the authors (K.K.) at the University of Tokyo Hospital. The other three underwent surgery by the other two authors and K.K as an assistant. Etiology of epilepsy was hemimegalencephaly in 4 patients who underwent surgery at 2, 4, 6 and 7 months old, perinatal injury in a patient who underwent surgery at 40 years old, post-vaccination status epilepticus in a patient who underwent surgery at 41 years old, and posttraumatic ulegyria in a patient who underwent surgery at 21 years old.

2.2. Preoperative evaluation

Indication for hemispherotomy was determined according to the preoperative workup including long-term video electroencephalography (EEG) monitoring, magnetic resonance imaging (MRI), 2-deoxy-2-[^{18}F]fluoro-D-glucose positron emission tomography, and magnetoencephalography. Developmental tests and neuropsychological tests were done in children and adults, respectively. For adult patients, language dominance was determined by Wada test, and residual motor function of the affected hemisphere was evaluated with somatosensory evoked potential and electromyogram evoked by transcranial magnetic simulation (Table 1).

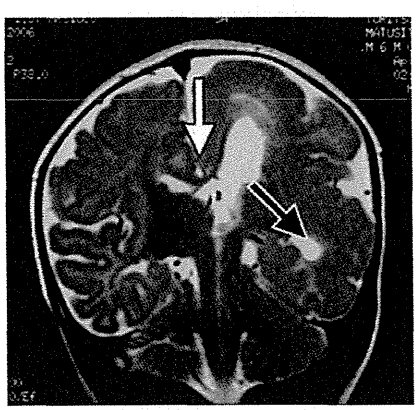

Fig. 1. Schematic image of the modification 1. Callosotomy was performed via an interhemispheric route. Head position, skin incision and craniotomy are the same as callosotomy that is routinely performed as a single surgical procedure. For our modified hemispherotomy, total callosotomy via an interhemispheric approach was first performed (white arrow). Then the lateral border of the thalamus is severed down to the inferior horn of the lateral ventricle (black arrow). When necessary, a small portion of the cingulate gyrus can be resected.

2.3. Surgical technique

We modified the Delalande's original vertical hemispherotomy in two aspects. Firstly, all procedures were done via an interhemispheric route instead of via a transcortical route (Fig. 1). Secondly, we set the anterior disconnection plane as the one that connects the anterior end of the choroidal fissure to the anterior end of the foramen of Monro, instead of the former to the subcallosal area (Fig. 2).

After induction of general anesthesia, patients' head were fixed in a median position with the vertex up. For adult patients, we used a three-point skeletal fixation device. For infants, we fixed their heads on a torus-shaped soft cushion covering them with plastic adhesive wound drapes. We used a U-shaped skin flap. Its anteriormost points were on the frontal hairline and the posteriormost point was a few centimeters behind the bregma. An approximately 7 × 5 cm craniotomy was made over the midline that was larger in the affected side. The dura was opened and reflected medially.

Following procedures were performed under the operative microscope. Firstly, we performed a complete callosotomy according to our routine procedure of callosotomy as a single treatment [8]. In brief, we carefully opened the interhemispheric cistern and exposed the whole length of the superior surface of the body of corpus callosum. The bridging veins were preserved as much as possible. Making the septum pellucidum as a guidance of midline, the corpus callosum was sectioned from the rostrum through the splenium. Then, via the same interhemispheric route, we opened the ependymal roof of the lateral ventricle on the affected side. The foramen of Monro and the choroid plexus that runs posterolaterally from the foramen to the ventricular trigone were visualized with retraction of the lateral wall of the ventricle. The disconnection plane of the projection fibers was the lateral border of the thalamus. Suction and cutting of the lateral border of thalamus was advanced anteriorly from the trigone to the anteriormost point of the choroidal fissure in the inferior horn of lateral ventricle. The choroid plexus in the inferior horn was a nice guidance in this process. Then, we cut the anterior border of the thalamus by connecting the resection from the anteriormost point of the choroidal

Please cite this article in press as: Kawai K et al. Modification of vertical hemispherotomy for refractory epilepsy. Brain Dev (2013), http://dx.doi.org/10.1016/j.braindev.2012.12.013

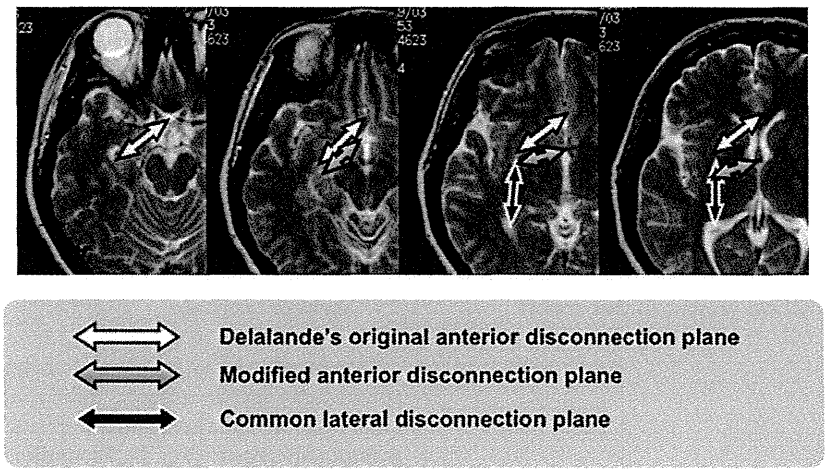

Fig. 2. Schematic image of the modification 2. The anterior disconnection plane as the one that connects the anterior end of the choroidal fissure to the anterior end of the foramen of Monro (gray arrow), instead of the former to the subcallosal area in the Delalande's original method (white arrow). Black arrow is the lateral disconnection plane common to the both methods.

Fig. 3. Serial images of postoperative MRI in the representative patients. (A) Two years after surgery in an infant with hemimegalencephaly. (B) Two days after surgery in an adult with hemiatrophy. In both patients, the corpus callosotomy was completely disconnected via an interhemispheric approach and the thalamus was completely disconnected by the minimal cutting plane. In A, a small part of the cingulate gyrus was resected to gain the lateral view.

fissure to the anteriormost point of the foramen of Monro. Thus disconnection of the projection fibers from the neocortices was completed. Finally, we cut the fornix, the projection fibers of the limbic system, at the ventricular trigone.

The lateral ventricle was rinsed and filled with the artificial cerebrospinal fluid. The roof of the lateral ventricle was closed with a gelatin sponge using fibrin glue. The dura, skull and skin were closed in a usual manner.

Please cite this article in press as: Kawai K et al. Modification of vertical hemispherotomy for refractory epilepsy. Brain Dev (2013), http://dx.doi.org/10.1016/j.braindev.2012.12.013

2.4. Postoperative evaluation

The completeness of disconnection of the affected hemisphere was evaluated in postoperative MRI. Disconnection lines were visually followed in each of three dimensional images. We checked particularly with care the complete sectioning of the genu and splenium of the corpus callosum, and the complete disconnection between the thalamus and surrounding cortices including the insula.

3. Results

Surgical procedure was completed without any intraoperative complication in all cases. Although we could obtain a good lateral view enough to vertically cut the lateral border of the thalamus in all patients, a small portion of the cingulate gyrus was excised in 2 infants with hemimegalencephaly to obtain a better view and a larger working space (Fig. 3). Postoperative course was uneventful in all patients. Blood loss during surgery was 50, 113, 136 and 150 mL in 4 infants and 160, 305 and 340 mL in 3 adults. No hypothalamic dysfunction including diabetes insipidus and poikilothermia was noted in any patients. There was no case that required transient CSF diversion or placement of CSF shunting. Seizure outcome was Engel's class I in 6 and class IV in 1. The patient whose outcome was class IV was hemimegalencephaly in whom postsurgical workup revealed residual epileptogenecity in the contralateral hemisphere.

Postoperative MRI revealed complete disconnection of affected hemisphere in all cases (Fig. 3).

4. Discussion

We reported our modification of Delalande's vertical hemispherotomy. While the original procedure devised by Delalande was an innovative procedure of hemispherotomy in minimizing brain resection [6], we thought that we could further improve it with minor modifications. One of the authors reviewed the hemispherotomy series at Tokyo Metropolitan Neurological Hospital for 37 children with malformation of cortical development [7]. In this study, the procedure was decomposed into a disconnection of the commissural fibers and a disconnection of the projection fibers, and elemental surgical procedures were compared in terms of the completeness of disconnection and the occurrence of complication (Fig. 4). For disconnection of the commissural fibers, we compared interhemispheric callosotomy used in two-stage hemispherotomy and transventricular callosotomy used in lateral hemispherotomy. Four of 19 cases of transventricular callosotomy were incomplete while none of 18 cases of interhemispheric callosotomy was incomplete. All of the four cases with incomplete transventricular callosotomy were hemimegalencephaly with the anomalous and asymmetric genu.

In Delalande's original method, callosotomy was performed in a parasagittal route that is similar to the interhemispheric route. Therefore, there may not be essential difference between our modification and Delalande's original, but we thought that staying in the midline decreased a risk of disorientation, particularly in anomalous midline structures often encountered in hemimegalencephaly, and particularly for surgeons who are used to interhemispheric callosotomy.

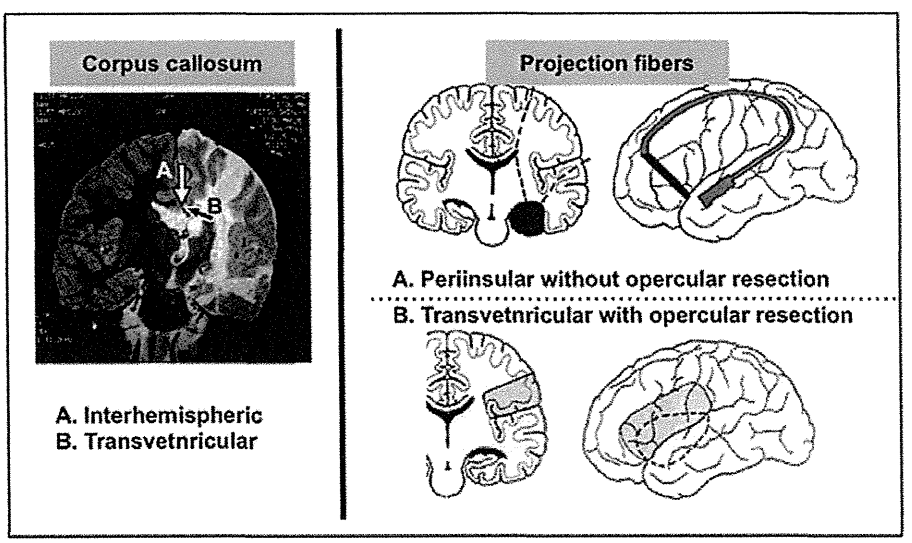

Fig. 4. The procedures of hemispherotomy are composed of disconnection of the corpus callosum and the projection fibers. For disconnection of the corpus callosum, interhemispheric callosotomy (left, A) and transventricular callosotomy (left, B) were compared. For disconnection of the projection fibers, periinsular hemispherotomy (right, A) and transopercular hemispherotomy (right, B) were compared.

Please cite this article in press as: Kawai K et al. Modification of vertical hemispherotomy for refractory epilepsy. Brain Dev (2013), http://dx.doi.org/10.1016/j.braindev.2012.12.013